Supporting Information

Engineering multi-component 3DOM $FeVCrO_x$ catalysts with high oxygen mobility for the oxidative dehydrogenation of 1-butene with CO_2

Xiaoshuai Gao[a, b], Weigao Han[b]*, Fang Dong[b], Xiaosheng Huang[b], Zhicheng Tang[b]*, Qiuye Li[a]*

([a] National & Local Joint Engineering Research Center for Applied Technology of Hybrid Nanomaterials, Henan University, Kaifeng 475004, China

[b] National Engineering Research Center for Fine Petrochemical Intermediates, State Key Laboratory for Oxo Synthesis and Selective Oxidation, Lanzhou Institute of Chemical Physics, Chinese Academy of Sciences, Lanzhou 730000, China)

*Corresponding author.

E-mail address: tangzhicheng@licp.cas.cn (Z. Tang), qiuyeli@henu.edu.cn (Q. Li)

Characterization of materials

Scanning electron microscope (SEM) images of three samples were obtained by a JSM-6701F cold field emission scanning electron microscope. The microstructure of the catalysts was observed by emission transmission electron microscopy (TEM). X-ray diffraction (XRD) analysis was conducted to explore the crystal phase of samples, which was recorded on a Rigaku D/MAX-RB X-ray diffractometer with Cu Kα radiation (λ = 1.5418 Å) and run in the range of 10-90° with 60 kV and 55 mA. Raman scattering was done by using a Laboratory Human Resources Evolution Raman spectrometer (BX41) with a 532 nm laser. Raman spectra were scanned in the range of 100 cm^{-1} to 2500 cm^{-1}. The XPS measurement was done on a VG ESCALAB 210 Electron Spectrometer (Mg Kα radiation; hν = 1253.6 eV) to determine the chemical states of elements in these samples. BET-related data were obtained by using an ASAP 2010 specific surface area analyzer at -196 ^oC. The crystalline phase analysis of the catalysts was performed on a Rigaku D/max-rb diffractometer using a CuK electrode (0.154 nm) with an instrument scan speed of 0.5^o/min and a scan angle range of 10^o to 90^o.

H_2-TPR, O_2-TPD, O_2-TPO, CO_2-TPD, and NH_3-TPD were done with a TP-5080-D Full-automatic Multifunctional Adsorption Apparatus Xianquan Co., LTD. instrument. The H_2-TPR test was performed on a fully automated multifunctional adsorption device (DAS-7000) with 0.05 g of catalyst in a quartz tube reactor. Pretreatment in N_2 atmosphere at 300 ^oC for 60 min. Then, the H_2/N_2 atmosphere (40 mL/min) was ramped up from 50 to 900 ^oC (10 ^oC /min). In the O_2-TPD test, 0.10 g of catalyst was placed in

a quartz tube reactor and pretreated at 300 °C under N_2 atmosphere for 1 h, followed by adsorption under N_2/O_2 atmosphere for 45 min, followed by purging under He atmosphere for 10 min (40 mL/min), and then heated at 40 to 900 °C at a rate of 10 °C /min. For the O_2-TPO test, all signals were detected by mass spectrometry (AMI-Master 400). First, 0.02 g catalysts were treated with 30ml min^{-1} N_2 at 150 °C for 1 h to remove the adsorbed gases. After cooling to 30 °C, 5% O_2 was induced. Once the mass signal stayed stable, the catalysts were heated to 900 °C with a ramping rate of 10 °C min^{-1}. The mass signal of H_2O (m/z = 18), CO (m/z = 28), O_2 (m/z = 32), and CO_2 (m/z = 44) were recorded. For the NH_3-TPD test, the difference from the O_2-TPD test is the pretreatment under N_2 atmosphere followed by adsorption under NH_3 atmosphere for 45 min and a final purge with N_2 for 10 min, followed by a purge with nitrogen at 40 mL/min for 10 min and heating from 40 to 900 °C at a rate of 10 °C/min. For CO_2-TPD, a 50 mg sample was pre-treated at an atmosphere of nitrogen. The temperature was increased from room temperature to 300 °C with a heating rate of 10 °C min^{-1}. And it was treated for 90 min. When it cooled down to room temperature, the temperature was increased from room temperature to 50 °C for 60 min with a gas of 5 % vol. CO_2 and 95 % vol. N_2 passing through. Finally, the temperature was increased from room temperature to 900 °C with a heating rate of 10 °C min^{-1}.

In situ diffuse reflectance infrared fourier transform spectroscopy (in situ DRIFTS) was collected on Bruker V70. The powder samples were degassed in N_2 gas with 25 mL/min gas volume at 400 °C for 30 min. After that, the samples were cooled to room temperature. Accordingly, a background spectrum was respectively gathered

at different temperatures (100 - 360 °C). 1-butene is introduced at 100°C for 30 min. To remove the weakly adsorbed 1-butene molecule, the samples were purged with He gas for another 30 min. Thereafter, a pure CO_2 gas (25 mL/min) were respectively introduced into the in suit cell to react with 1-butene as requires. Finally, the samples were further heated to different temperatures (100 - 360 °C) to collect the corresponding spectra, respectively.

The in situ DRIFTS in the case of water are consistent with the above parameters. The difference is that the water was brought into the in-situ cell by flowing carbon dioxide (25 ml/min) into the tank with water.

1-Butene conversion is described as:

$$[C]_{1\text{ - Butene}} = \frac{[C]\text{inlet - }[C]\text{outlet}}{[C]\text{inlet}} \times 100\%$$

The BD selectivity is described as:

$$[S]_{BD} = \frac{[C]_{BD}}{[C]_{inlet} - [C]_{outlet}} \times 100\%$$

The definition of the yield of BD is:

$$[Y]_{BD} = \frac{[C]_{BD}}{[C]_{inlet}} \times 100\%$$

CO_2 utilization is defined as:

$$[U]_{CO2} = \frac{[C]_{CO2}\text{inlet - }[C]_{CO2}\text{outlet}}{[C]_{CO2}\text{inlet}} \times 100\%$$

The formula for the 1-butene reaction rate is as follows:

$$r = \frac{cXF}{Vm}$$

Where *r, c X, F, V*, and *m* represent 1-butene reaction rate, 1-butene concentration, 1-butene conversion ratio, gas volume flow rate, molar volume of gas, and catalyst quality, respectively.

Classification of different reactions

The oxidative dehydrogenation of butene is a complex process that might involve multiple reactions. After analyzing the converted butene and the products, four possible reactions (dehydrogenation, coking, cracking and isomerization) have been identified. The butene conversion rate is made up of these reactions together and could be represented by the eight reaction equations outlined below:

1. Dehydrogenation reactions,

$C_4H_8 \rightarrow C_4H_6 + H_2$ *Eq.* (1)

$C_4H_8 + CO_2 \rightarrow C_4H_6 + CO + H_2O$ *Eq.* (2)

2. Coking reaction,

$C_4H_8 \rightarrow 4C + 4H_2$ *Eq.* (3)

3. Cracking reactions,

$C_4H_8 + H_2 \rightarrow CH_4 + C_3H_6$ *Eq.* (4)

$C_4H_8 + H_2 \rightarrow C_2H_6 + C_2H_4$ *Eq.* (5)

$2C_4H_8 + 2H_2 \rightarrow 2C_3H_8 + C_2H_4$ *Eq.* (6)

4. Isomerization Reaction

1- $C_4H_8 \rightarrow$ cis-2- C_4H_8 *Eq.* (7)

1- $C_4H_8 \rightarrow$ trans-2- C_4H_8 *Eq.* (8)

The corresponding conversion rate is calculated by the following formula:

$$Conversion_{dehydrogenation} = Yield_{BD}$$

$$Conversion_{coking} = Conversion_{butene} \times \frac{1}{4} \times \frac{\sum m_i \times n_{i,in} - \sum m_i \times n_{i,out}}{n_{butene,in} - n_{butene,out}}$$

$$Conversion_{isomerization} = Yield_{cis\text{-}2\text{-}BD} + Yield_{trans\text{-}2\text{-}BD}$$

$$Conversion_{Cracking} = Yield_{methane} + Yield_{ethane} + Yield_{propane}$$

Carbon balance

The carbon balance is calculated according to the following equation:

$$\text{Carbon balance}(\%) = \frac{\Sigma m_i \times n_{i,out}}{\Sigma m_i \times n_{i,in}} \times 100\%$$

Where $n_{i,in}$ and $n_{i,out}$ are the molar quantity of the carbonaceous compounds (such as C_4H_8, CO_2, CH_4, and CO) at inlet and outlet, respectively. m_i correspond to the number of carbon atoms.

Table S1 Oxidative dehydrogenation performance of Fe-based catalysts.

Sample	Feedstock	Conversion	Selectivity	Yield	CO_2 utilization	Ref.
2V–Fe/KIT-6	propane	37.8 % (Propane)	87.0 %	32.9%	18.5 %	1
5Fe-5V-Al_2O_3	propane	41.3 % (Propane)	84.4 %	30.5 %	——	2
Fe/S-1-E-EDA	Isobutane	21.3 % (Isobutane)	53.4 %	——	17.9 %	3
Ni_3Fe_1/CeO_2	n-butane	30.9 % (n-butane)	4.1 %	1.4 %	59.3 %	4
Fe_2O_3/Meso-CeAl-100	n-butene	85 % (1-butene)	51 %	——	14 %	5

Table S2 Composition of samples.

Sample	NH_4VO_3 (Molecular weight: 116.98)	$Cr(NO_3)_3·9H_2O$ (Molecular weight: 400.14)	$Fe(NO_3)_3·9H_2O$ (Molecular weight: 404.00)	$C_9H_{21}AlO_3$ (Molecular weight: 204.24)	V/Fe (Mole ratio)	Cr/Fe (Mole ratio)
$FeVAlO_x$	0.06 g	———	2.02 g	2.04 g	0.1	———
$FeVCrAlO_x$	0.06 g	0.20 g	2.02 g	2.04 g	0.1	0.1
$FeVCr_2AlO_x$	0.06 g	0.40 g	2.02 g	2.04 g	0.1	0.2
$FeVCr_3AlO_x$	0.06 g	0.60 g	2.02 g	2.04 g	0.1	0.3
$FeCrAlO_x$	———	0.20 g	2.02 g	2.04 g	———	0.1
$FeVCrAlO_x$	0.06 g	0.20 g	2.02 g	2.04 g	0.1	0.1
$FeCrV_2AlO_x$	0.12 g	0.20 g	2.02 g	2.04 g	0.2	0.1
$FeCrV_3AlO_x$	0.18 g	0.20 g	2.02 g	2.04 g	0.3	0.1

Table S3 The H_2-TPR peak area of the $FeVAlO_x$, $FeCrAlO_x$, $FeVCrAlO_x$, FeV_2CrAlO_x, FeV_3CrAlO_x samples.

Samples	peak area (a.u.)
$FeVAlO_x$	7506
$FeCrAlO_x$	8394
$FeVCrAlO_x$	8946
FeV_2CrAlO_x	9479
FeV_3CrAlO_x	10157

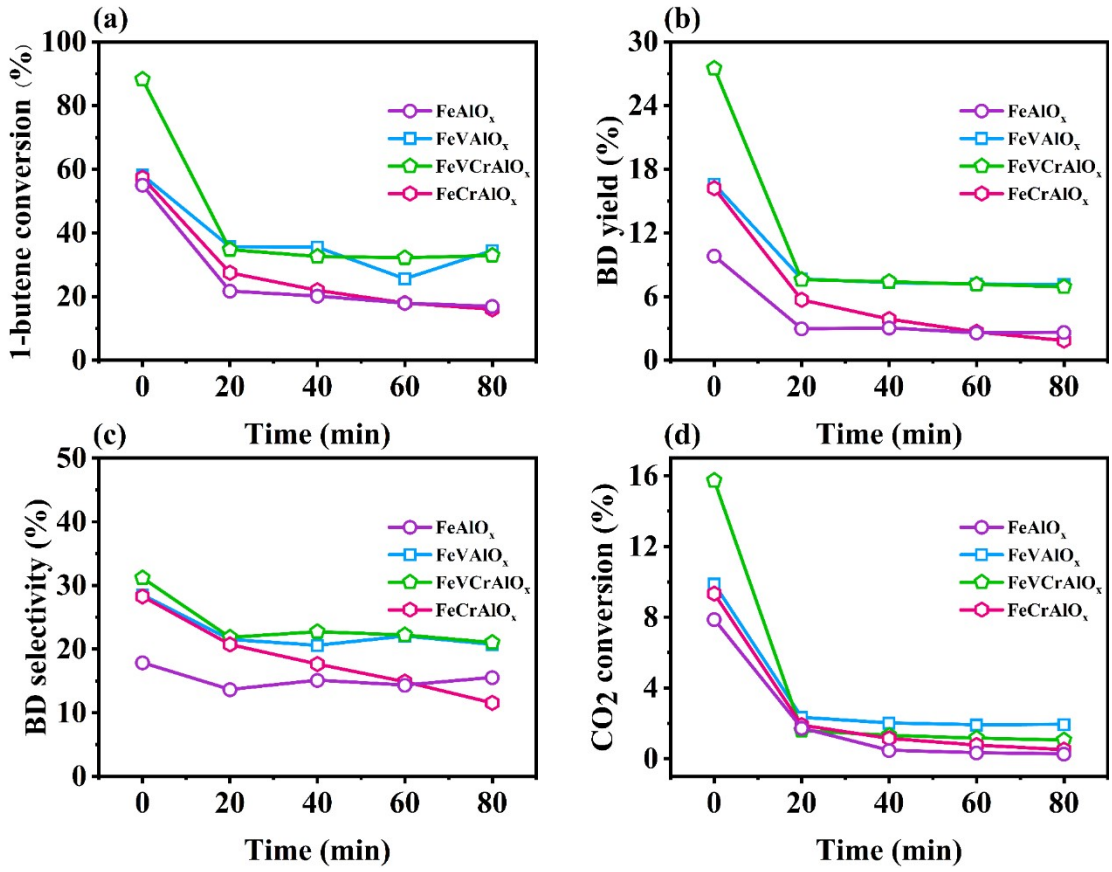

Fig. S1. The comparative activity of $FeAlO_x$, $FeVAlO_x$, $FeCrAlO_x$, and $FeVCrAlO_x$ catalysts.

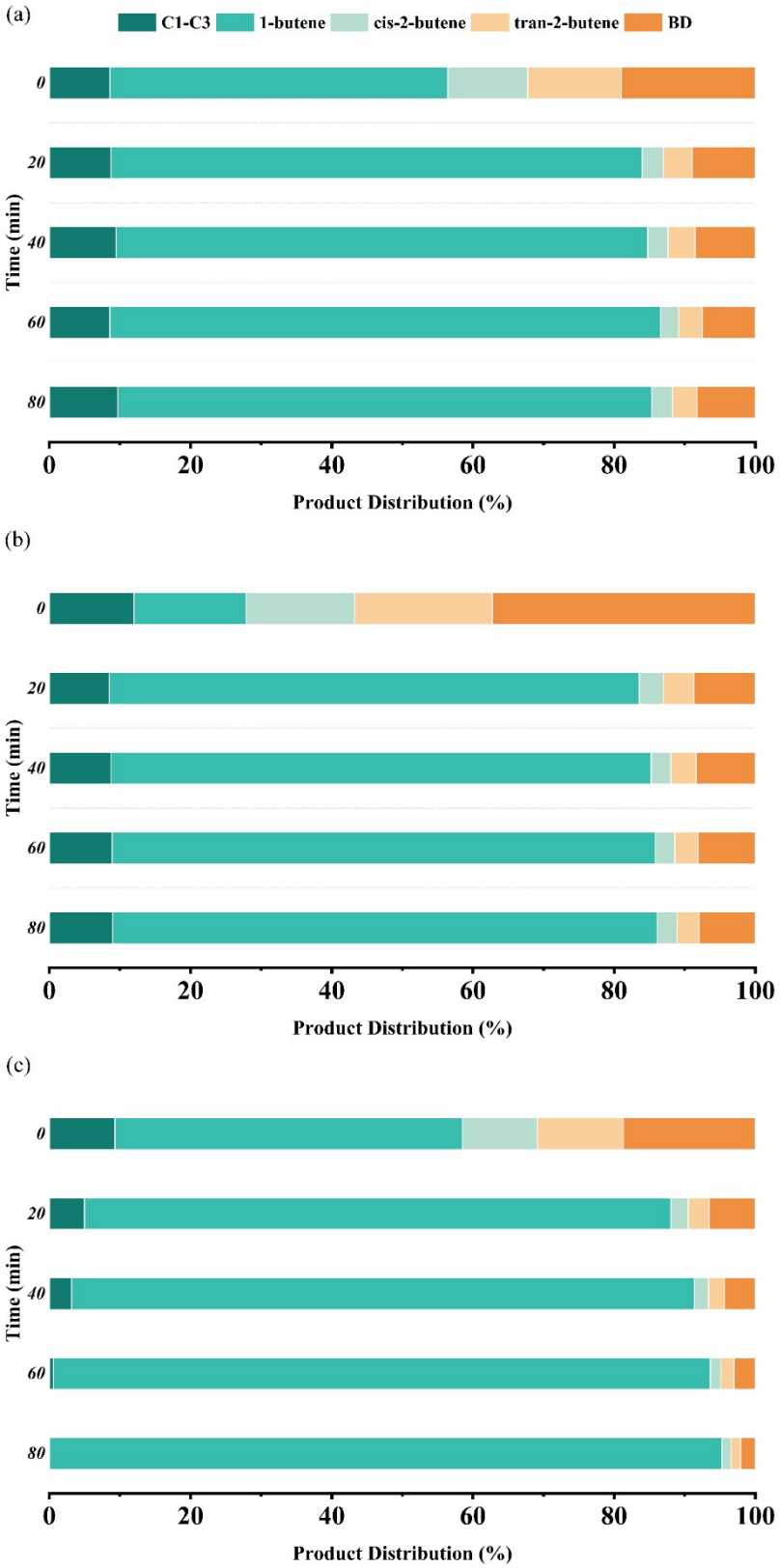

Fig. S2. The product distribution with different catalysts. (a) $FeVAlO_x$ (b) $FeVCrAlO_x$ (c) $FeCrAlO_x$.

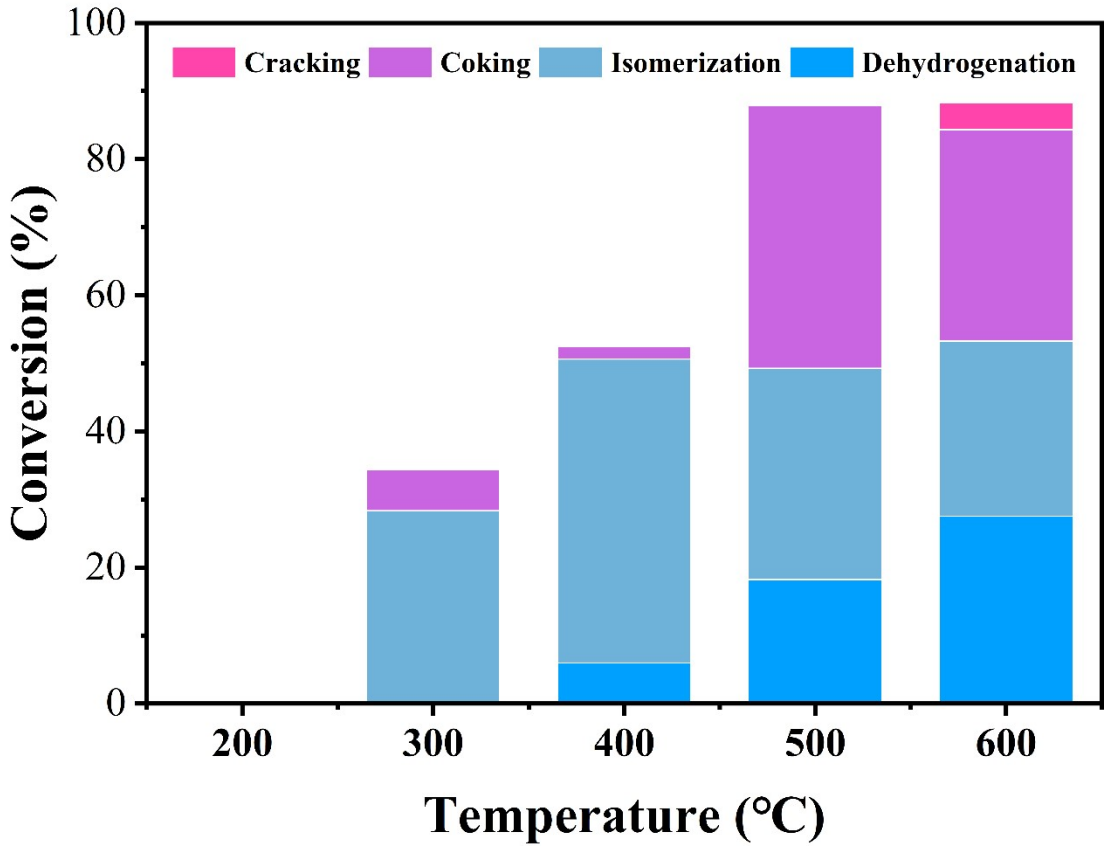

Fig. S3. The relationship between the conversion rates of various reactions (Cracking, Coking, Isomerization, and Dehydrogenation) and temperature on $FeVCrAlO_x$.

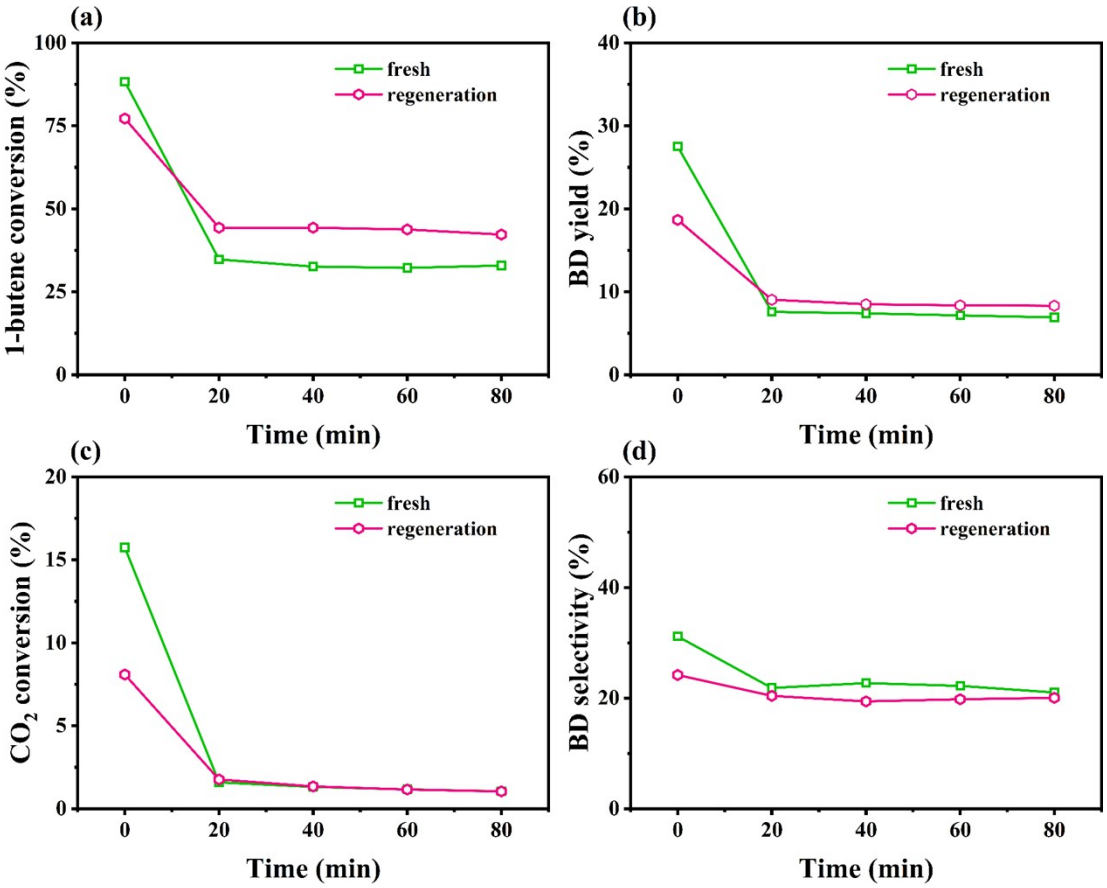

Fig. S4. The comparison of catalyst activity before and after regeneration on $FeVCrAlO_x$ catalyst: (a) 1-butene conversion, (b) BD yield, (c) CO_2 conversion, (d) BD selectivity.

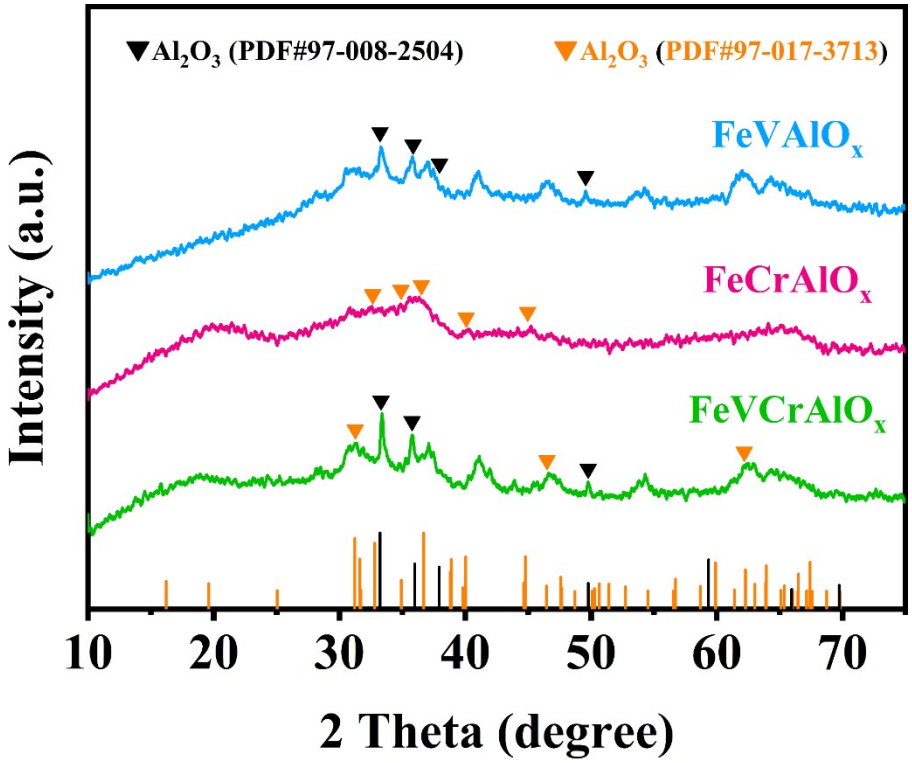

Fig. S5. XRD patterns of the $FeVAlO_x$, $FeCrAlO_x$ and $FeVCrAlO_x$, samples.

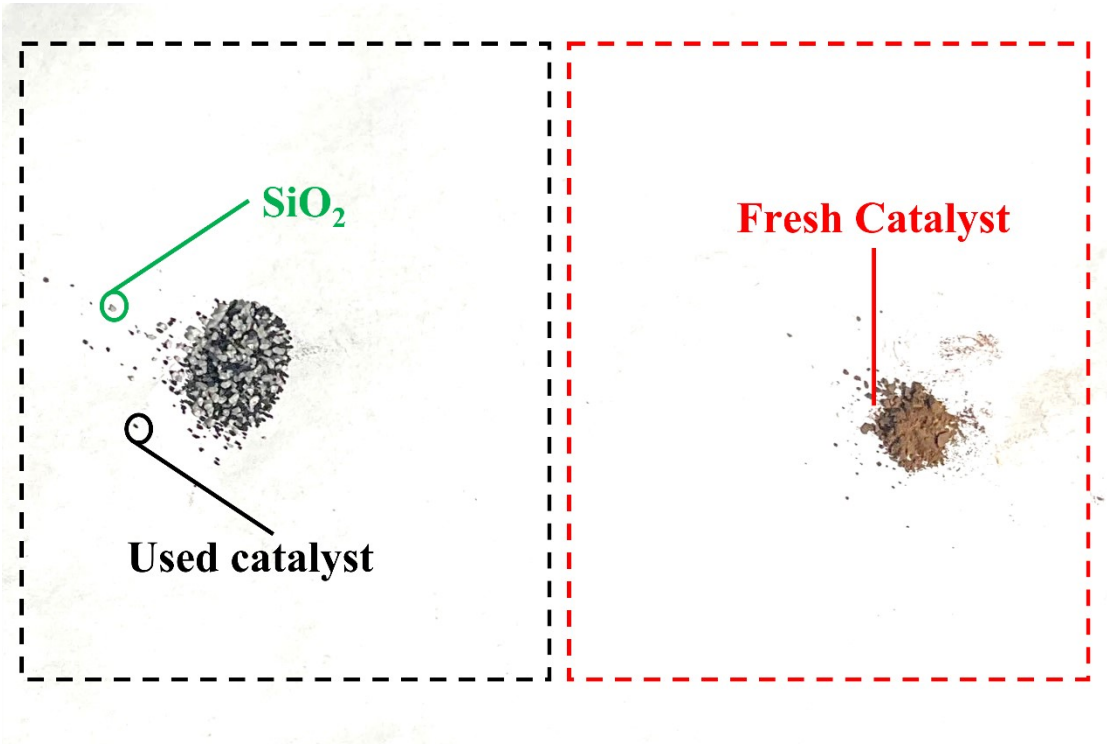

Fig. S6. Catalyst morphology before and after reaction.

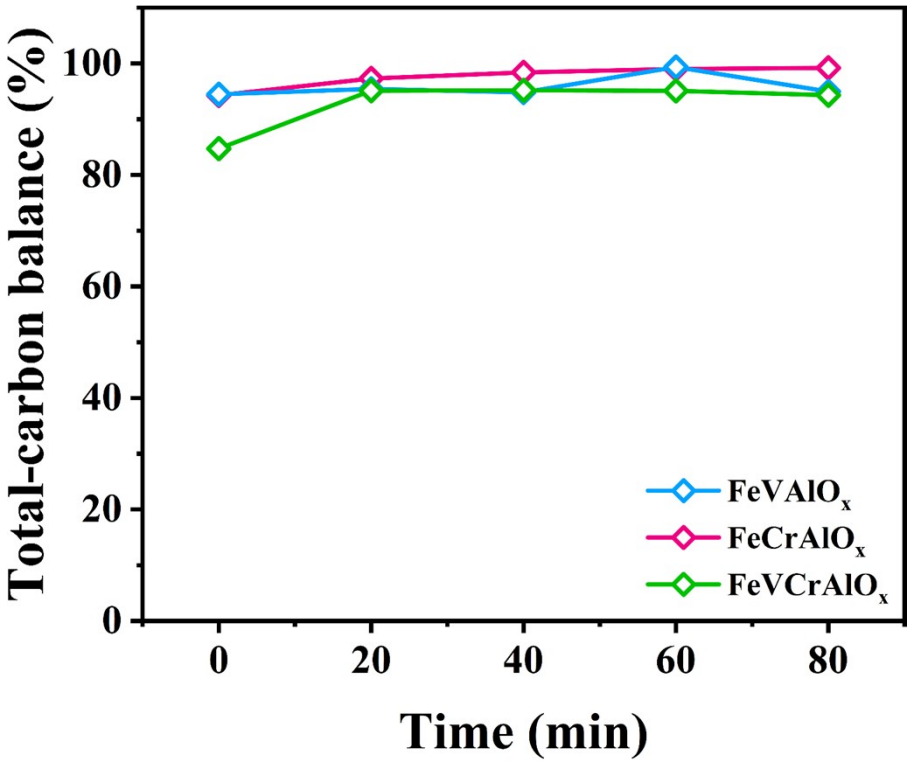

Fig. S7. Carbon balance of different catalysts.

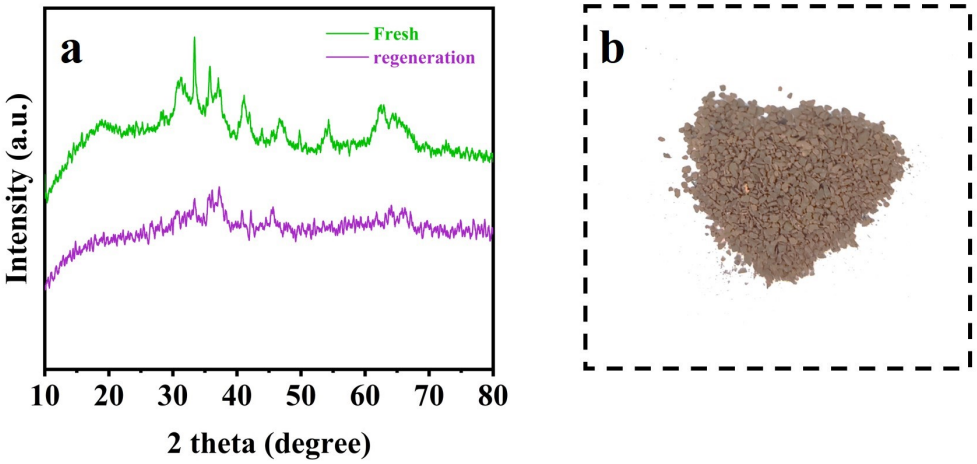

Fig. S8 XRD of regenerated catalyst (a) and surface analysis of sample (b).

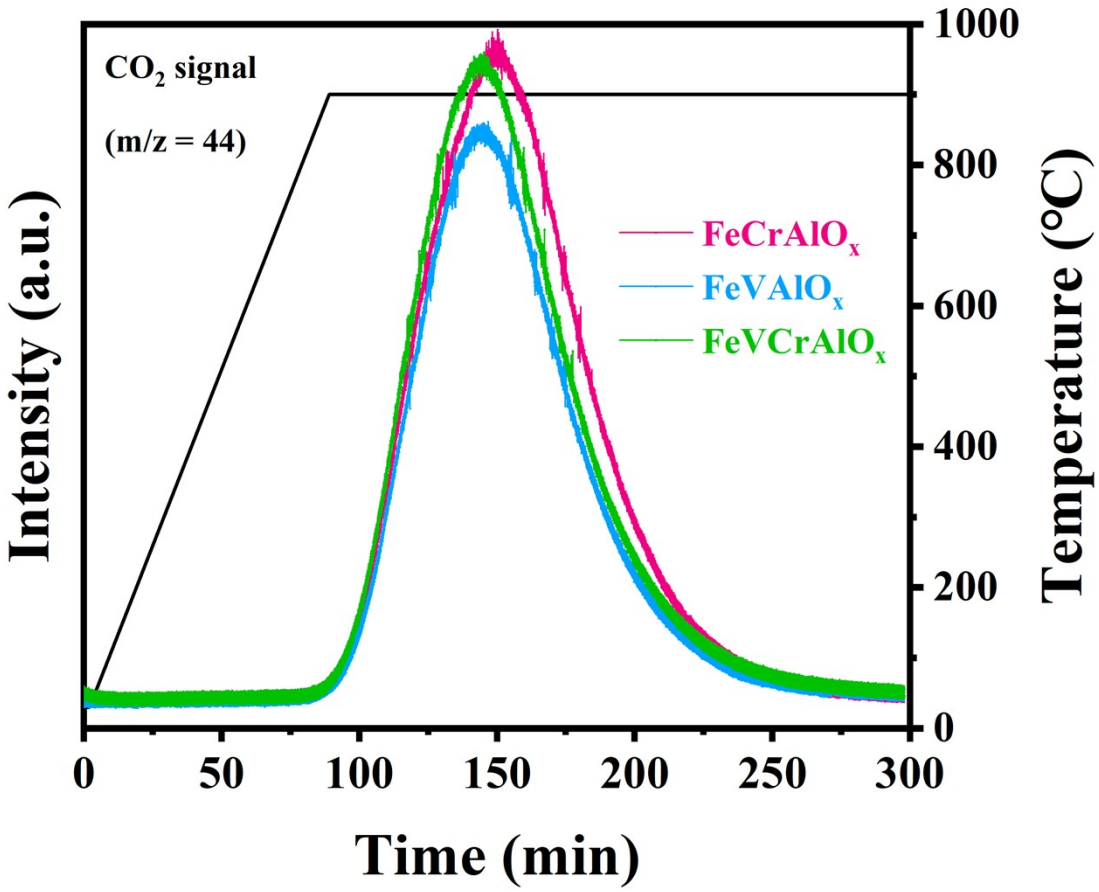

Fig. S9. O_2-TPO data of the used catalysts ($FeVAlO_x$, $FeCrAlO_x$, $FeVCrAlO_x$) with CO_2 mass signal (m/z=44) recorded.

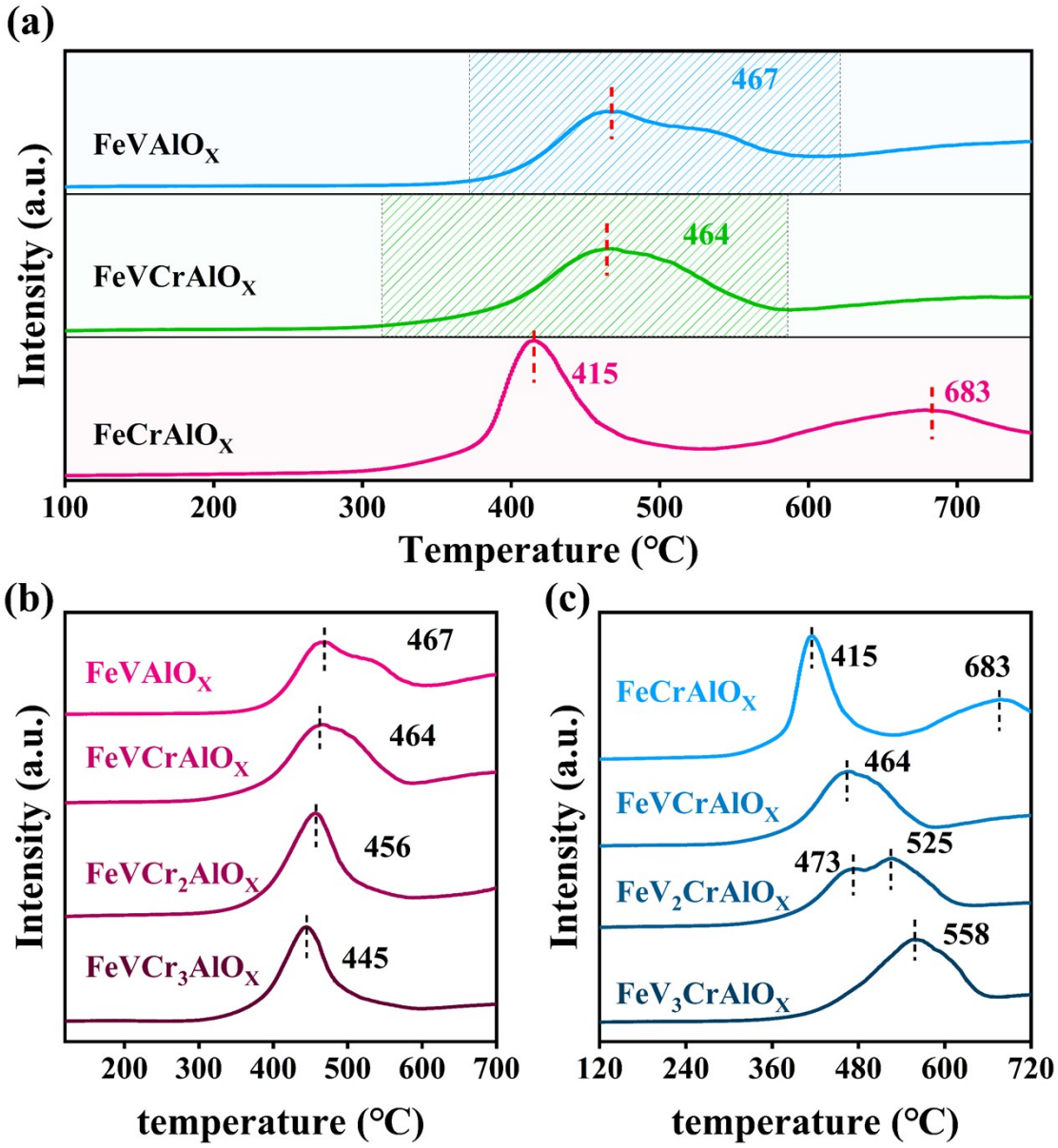

Fig. S10. H_2-TPR curves of the $FeVAlO_x$, $FeCrAlO_x$, $FeVCrAlO_x$ (a), and H_2-TPR curves of catalysts with different Cr (a) and V (b) contents.

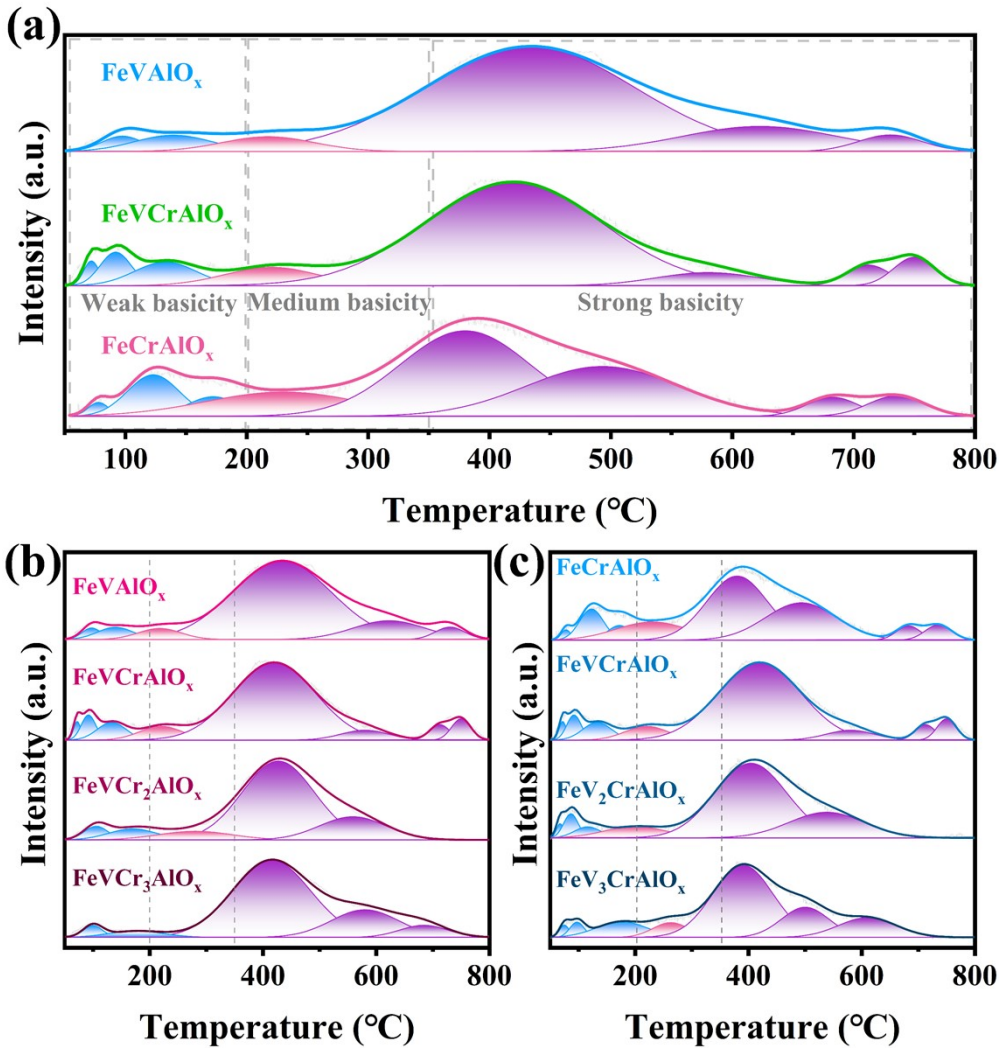

Fig. S11. CO_2-TPD curves of the $FeVAlO_x$, $FeCrAlO_x$, $FeVCrAlO_x$ (a), and the curves of catalysts with different Cr (a) and V (b) contents.

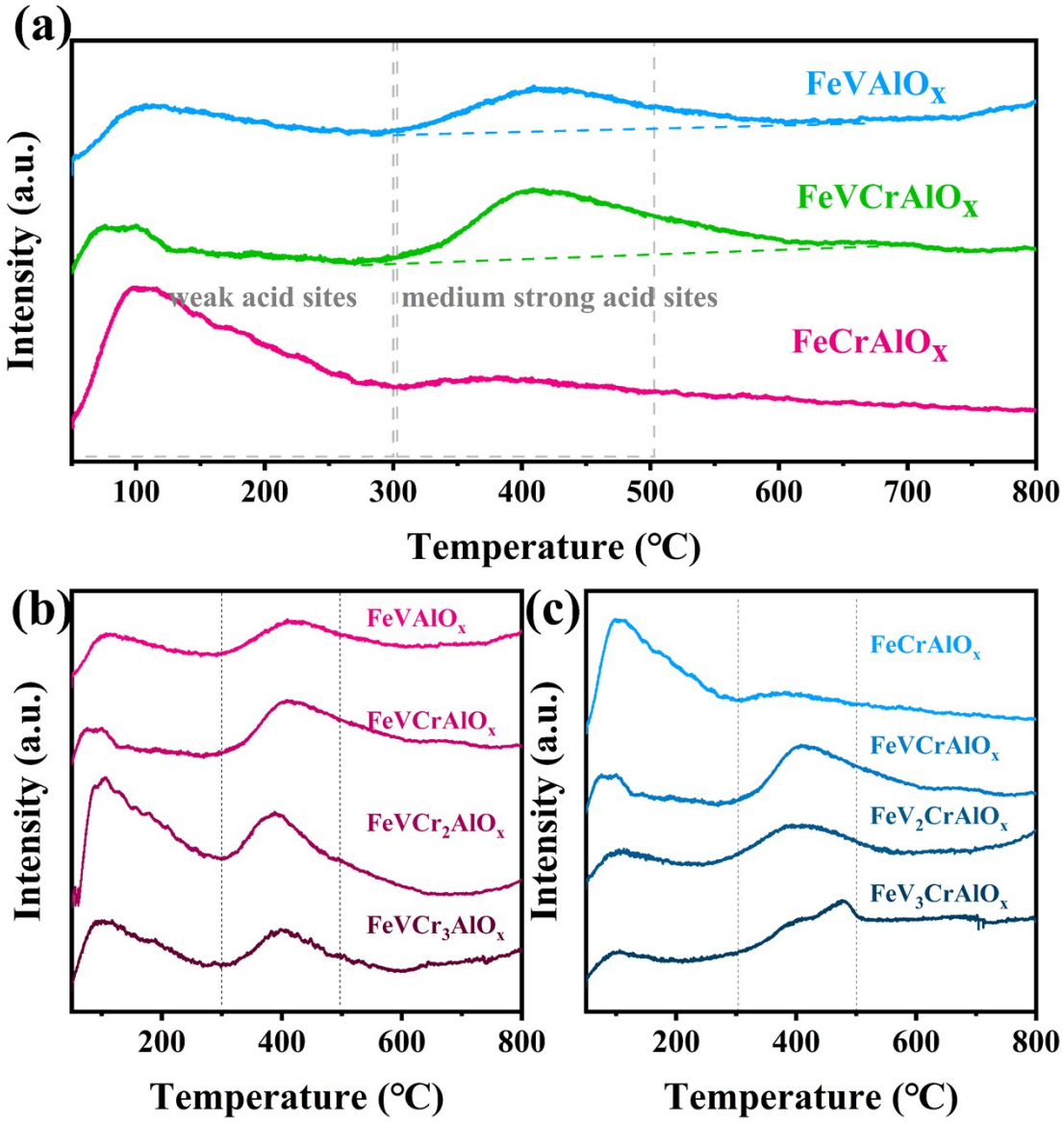

Fig. S12. NH_3-TPD curves of the $FeVAlO_x$, $FeCrAlO_x$, $FeVCrAlO_x$ (a), and the curves of catalysts with different Cr (b) and V (c) contents.

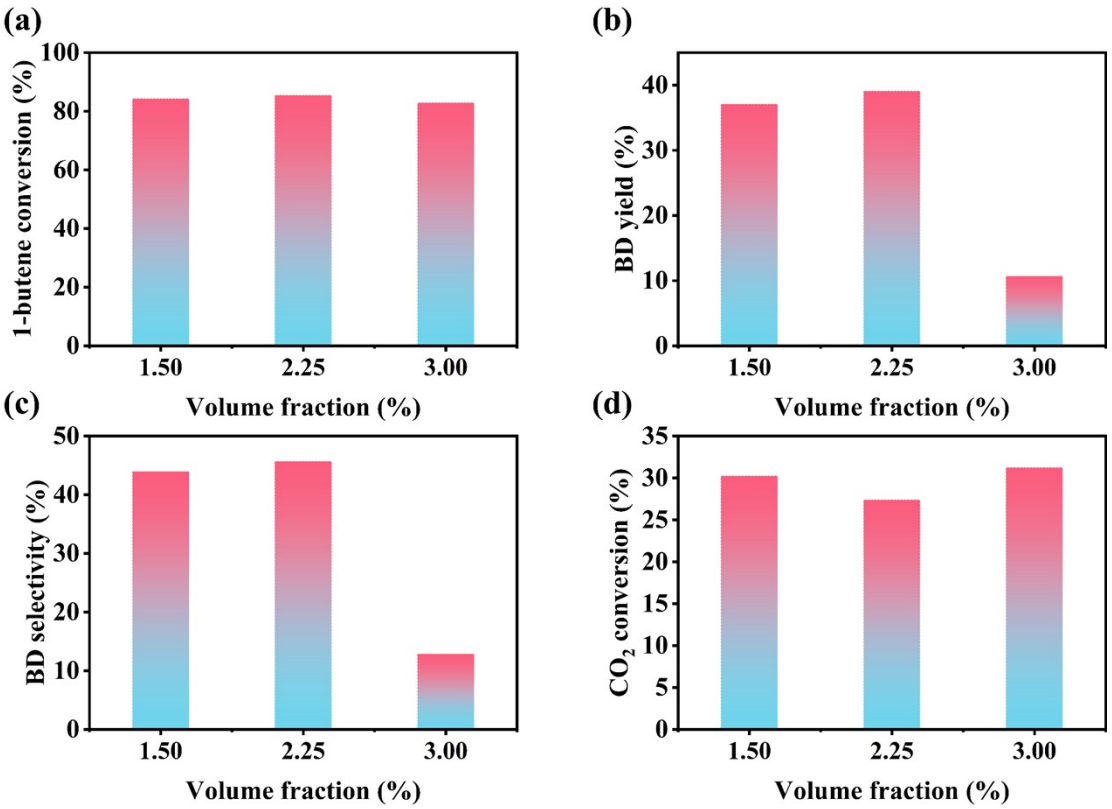

Fig. S13. Catalytic activity of $FeCrAlO_x$ samples in different water volume fractions at 600 ℃. (a) 1-butene conversion. (b) BD yield, (c) BD selectivity, and (d) CO_2 conversion.

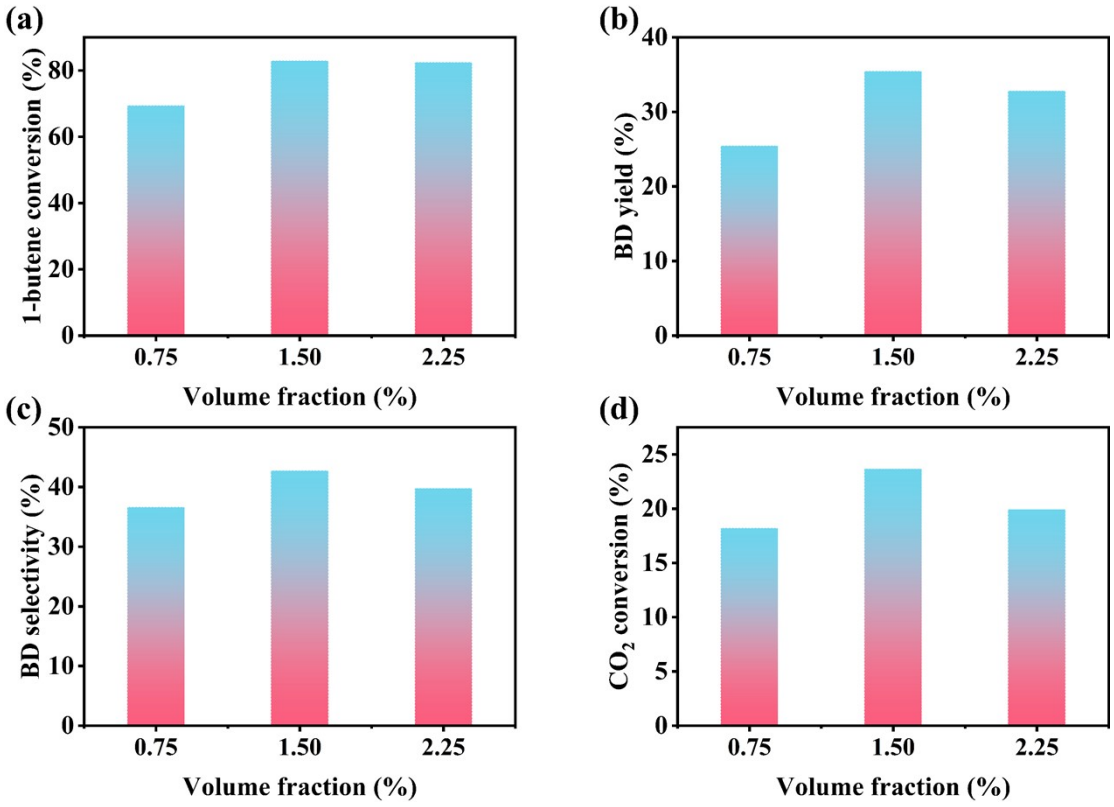

Fig. S14. Catalytic activity of $FeVAlO_x$ samples in different water volume fractions at 600 ℃. (a) 1-butene conversion. (b) BD yield, (c) BD selectivity, and (d) CO_2 conversion.

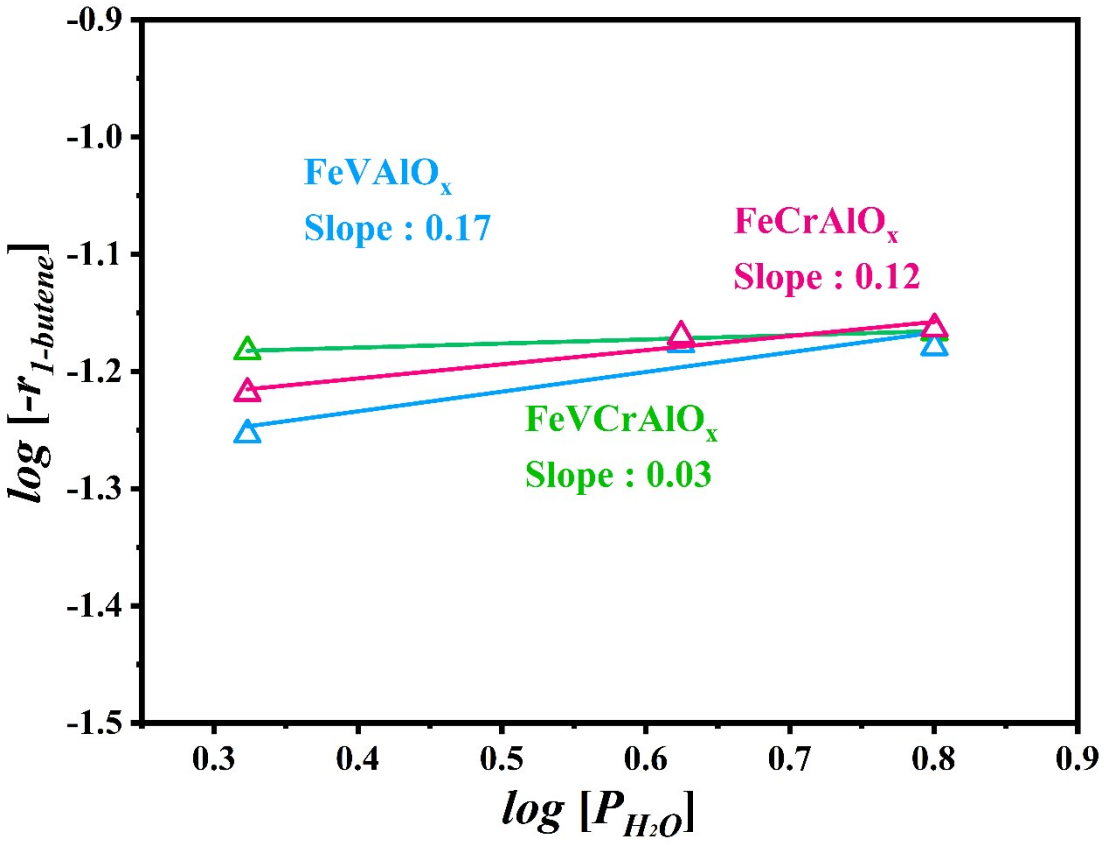

Fig. S15. Reaction orders concerning $FeVAlO_x$, $FeCrAlO_x$, and $FeVCrAlO_x$ samples, for 1-butene consumption in the presence of water.

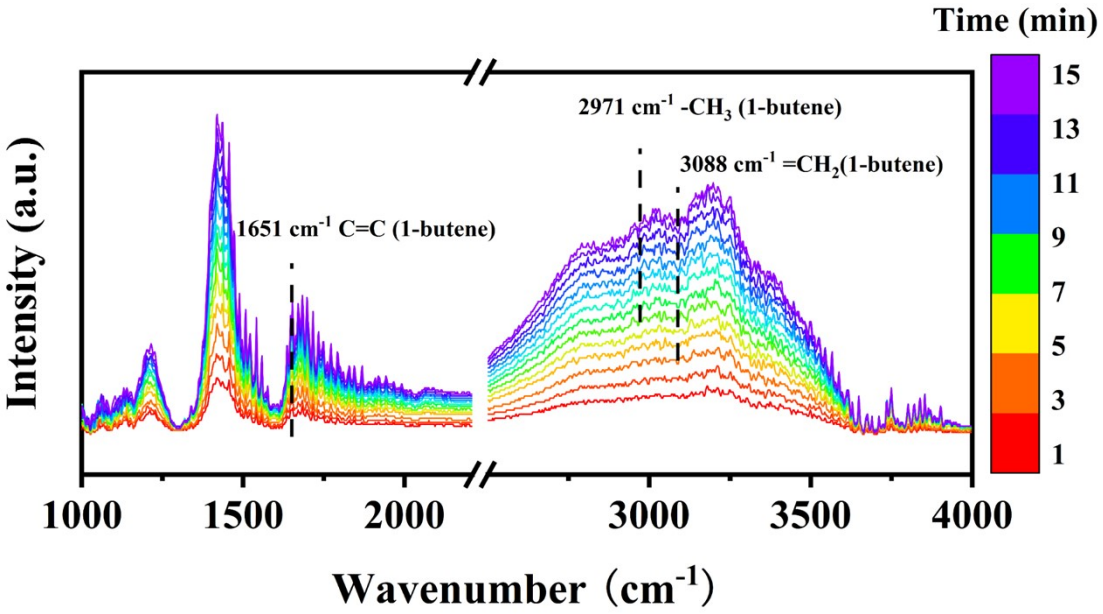

Fig. S16. In situ DRIFTs spectra of 1-butene adsorption at 100 ℃ over the $FeVCrAlO_x$ samples.

Reference：

1. R. Liu, F. Zha, H. Tian, X. Tang, Y. Chang, X. Guo, Coupling of Propane with CO_2 to Propylene Catalyzed by V–Fe Modified KIT-6 Zeolites, Catal Surv Asia., 2021, 25, 406-418.
2. S. Zhang, C. Zhou, S. Wang, Z. Qin, G. Shu, C. Wang, L. Song, L. Zheng, X. Wei, K. Ma, H. Yue, Facilitating CO_2 dissociation via Fe doping on supported vanadium oxides for intensified oxidative dehydrogenation of propane, Chem. Eng. J., 2024, 481, 148231.
3. J. Wang, M. Liu, J. Li, C. Wang, X. Zhang, Y. Zheng, X. Li, L. Xu, X. Guo, C. Song, X. Zhu, Elucidating the Active-Phase Evolution of Fe-Based Catalysts during Isobutane Dehydrogenation with and without CO_2 in Feed Gas, ACS Catal., 2022, 12, 5930-5938.
4. X. Li, B. Yan, S. Yao, S. Kattel, J.G. Chen, T. Wang, Oxidative dehydrogenation and dry reforming of n-butane with CO_2 over NiFe bimetallic catalysts, Appl. Catal. B: Environ., 2018, 231, 213-223.
5. B. Yan, B. Wang, L. Wang, T. Jiang, Ce-doped mesoporous alumina supported Fe-based catalyst with high activity for oxidative dehydrogenation of 1-butene using CO_2 as soft oxidant, J. Porous Mat., 2019, 26, 1269-1277.